Kinetic Study of Carbon Nanotubes Synthesis by Fluidized Bed Chemical Vapor Deposition

R. Philippe
LCC/ENSIACET/INPT, UPR CNRS 8241, Toulouse University, 31077 Toulouse Cedex 4, France
ARKEMA LACQ Research Center, 64170 Lacq, France

Ph. Serp and Ph. Kalck
LCC/ENSIACET/INPT, UPR CNRS 8241, Toulouse University, 31077 Toulouse Cedex 4, France

Y. Kihn
CEMES—CNRS UMR 8011, 31055 Toulouse, France

S. Bordère, D. Plee, and P. Gaillard
ARKEMA LACQ Research Center, 64170 Lacq, France

D. Bernard
ARKEMA, 92705 Colombes Cedex, France

B. Caussat
LGC/ENSIACET/INPT, UMR CNRS 5503, 31106 Toulouse Cedex 1, France

Multi-walled carbon nanotubes (MWCNTs) have been produced with high selectivity by fluidized bed catalytic chemical vapor deposition from ethylene on Fe/Al_2O_3 catalysts. The influence of operating parameters such as deposition duration, temperature, ethylene and hydrogen partial pressures, and iron loading on MWCNT productivity, process selectivity, characteristics of final powders, and chemical composition of the outlet gases has been analyzed. Using gas phase chromatography, methane and ethane have been detected, whatever are the conditions used. Between 650 and 750°C, no catalyst deactivation occurs because nucleation remains active all along the synthesis, thanks to the explosion of the catalyst grains. Above 650°C, ethane itself produces MWCNTs, whereas methane does not react in the temperature range, 550–750°C. The formation of MWCNTs induces marked bed expansions and sharp decreases of grain density. Apparent kinetic laws have been deduced from the collected data. The apparent partial orders of reaction for ethylene, hydrogen, and iron were found to be 0.75, 0, and 0.28, respectively. © 2008 American Institute of Chemical Engineers *AIChE J*, 55: 450–464, 2009
Keywords: multi-walled carbon nanotubes, catalytic CVD, fluidized bed, kinetic study, iron catalyst, ethylene

Introduction

Multi-walled carbon nanotubes (MWCNTs) are now expected to bring significant breakthroughs in various fields including (i) engineering materials, as additives for polymers

or coating to enhance electrical or mechanical properties, (ii) energy, as components of supercapacitors, fuel cells, or batteries, and (iii) catalysis and sensors. For mass production of MWCNTs, the most promising route is fluidized bed catalytic chemical vapor deposition (FB-CCVD), thanks to the technology robustness, to the high productivity it permits to achieve, especially if organized in continuous mode, and to the resulting potential cheapness of the MWCNTs produced.[1–5] This process consists in putting into contact a catalytic powder with a hydrocarbon gaseous source under appropriate conditions of temperature, pressure, and gas flow rates, so that a vigorous mixing of the particles is generated by the gas flow. This fluidized state naturally leads to intense thermal and mass transfers, which are necessary to reach highest carbon yield, catalyst efficiency, product homogeneity, and selectivity in MWCNTs.[1,3,4]

The synthesis of carbon nanotubes (CNTs) by heterogeneous CCVD involves the catalytic decomposition of a carbon source (a hydrocarbon, CO, or an alcohol) on nanostructured transition metal supported catalysts as Co, Ni, or Fe[6] supported on inert powders such as Al_2O_3, SiO_2, or MgO. The process and the MWCNT characteristics are highly sensitive to the synthesis conditions, including catalyst features, nature of the carbon source, temperature, reactant concentration, gas flow rate, and run duration.[7,8] Obviously, the understanding and the mastery of these parameters are of relevant importance to develop an optimized process for large-scale production. This explains why several studies deal with experimental kinetic analyses of each operating parameter for a given catalytic powder/carbon source couple. To the best of our knowledge, Zavarukhin and Kuvshinov[9] and our group[3] are the sole to have conducted such a study in a fluidized bed reactor. Zavarukhin and Kuvshinov[9] focused on the synthesis of carbon nanofibers from methane using Ni/Al_2O_3 catalysts. They developed a kinetic model accounting for their main experimental observations, that is, catalyst deactivation with run duration and increase in nanofibers productivity with temperature. Morançais et al.[3] performed a parametric study on the influence of temperature, run duration, total pressure, and composition of the gaseous phase on MWCNT formation from ethylene, hydrogen, and nitrogen mixtures using Fe/Al_2O_3 catalysts. They report a kinetic law with a positive order with respect to ethylene concentration and a process limitation due to internal diffusion in the porosity of catalyst grains. Furthermore, the works of Gommes et al.[10] and Pirard et al.[8] concern a kinetic study on MWCNT formation from ethylene mixed with hydrogen or helium using Fe-Co/Al_2O_3 catalysts. They connected a mass spectrometer to their horizontal fixed bed reactor (quartz boat). Gommes et al. performed a blank experiment at 700°C proving that without catalyst, no ethylene decomposition occurred. Gommes et al.[10] as Pirard et al.[8] found that in the presence of a catalyst, hydrogen is produced and that the total number of molecules increase because of the reaction. As a consequence, the sole reactions considered in their study focused on the formation of MWCNTs and hydrogen. Gommes et al.[10] determined a reaction order of 1 for ethylene, for inlet molar fractions of C_2H_4 lower than 0.3 at 700°C. For Pirard et al.,[8] the ethylene partial order was between 0 and 1, and increased from 600 to 700°C, whereas the hydrogen partial order was close to zero. They found activation energy for MWCNT synthesis close to 135 kJ/mol, which is close to the activation energy for carbon diffusion into bulk γ-Fe.[11] Some authors[12,13] have used a microbalance to achieve a continuous control of CNT synthesis in real time. Thus, Perez-Cabero et al.[12] studied the influences of temperature and of acetylene and hydrogen partial pressures during MWCNT formation using Fe/SiO_2 catalysts. They found that MWCNT productivity increased with time between 700 and 800°C, whereas a partial deactivation was observed between 600 and 700°C. A high partial pressure of hydrogen provided competitive reactions of hydrogenation leading to a parasitic consumption of acetylene. Additionally, Svreck et al.[13] analyzed the influences of run duration and of the ethane/hydrogen ratio on the formation of MWCNTs from C_2H_6/H_2/He mixtures on Fe/Al_2O_3 catalysts. They found a dependence of the nanotubes formation rate in $(P_{C2H6}/P_{H2})^{1/2}$. They evidenced a first step of MWCNT growth on the surface of the catalyst grains and then a second step in the core of the grains. A similar behavior was reported by Morançais et al.[3]

In this work, a kinetic study is presented concerning MWCNT synthesis by FB-CCVD using ethylene as carbon source and Fe/Al_2O_3 powders as catalysts. The influence of the main synthesis conditions on MWCNT productivity, process selectivity, and characteristics of the final powders, as its density and mean diameter is reported. Using gas phase chromatography (GC), the concentration of the outlet gases has also been measured in running conditions for the whole experiments performed to develop original apparent kinetic laws.

Experimental

The experimental set up employed is schematically presented in Figure 1. The FB reactor is entirely constructed from a 304L stainless steel; its dimensions are 5.3 cm internal diameter and 1 m height. The gas distributor is a stainless steel perforated plate covered with a stainless steel grid supplied with 50 μm holes, and a two-zone electric furnace allows monitoring the FB temperature via two thermocouples fixed on the outer reactor walls. Electronic grade ethylene, hydrogen and nitrogen gases (Air Liquide) are supplied to the reactor through mass flow meters. A pressure sensor allows measuring the differential pressure drop between the bottom and the top parts of the reactor. Three thermocouples are placed into the FB at various axial positions to monitor the temperature. After its exit from the reactor, the gaseous effluents flow through a bag filter, to collect elutriated particles or fines that could be formed during the experiments. The chemical composition of the outlet gas flow has been measured by gas phase chromatography (GC Clarus 500 Perkin Elmer) associated to a TotalChrome workstation; gas sampling was performed every 10 min via a micro pump (LFS-113D Gilian). A DasyLab® system enabled the on-line acquisition of the differential pressure and FB temperatures.

The catalyst support consists in mesoporous alumina (γ-Al_2O_3) particles; it is previously treated in another reactor to obtain under nominal conditions, a 10% Fe/Al_2O_3 w/w catalyst. The catalytic powder has a mean volume diameter of 322 μm, a Sauter diameter of 298 μm and a minimum fluidization velocity U_{mf} at 650°C of 3.5 cm/s. More details concerning the catalyst preparation are available elsewhere.[14]
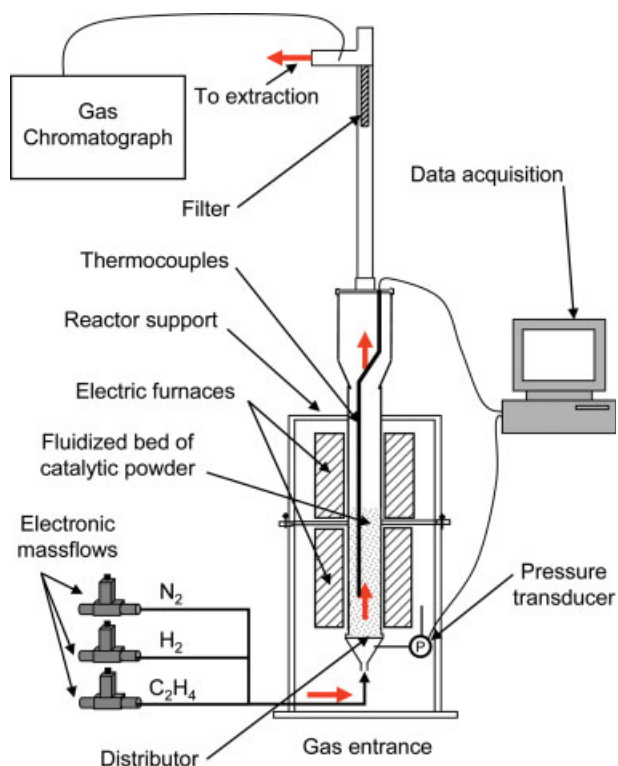
Figure 1. Schematic representation of the experimental set up.

[Color figure can be viewed in the online issue, which is available at www.interscience.wiley.com.]

The operating parameters examined are given in Table 1. First, on the basis of some literature results[4,10] and after preliminary experiments, nominal operating conditions have been chosen corresponding to run Cin3 of Table 1. The weight of catalytic powders has been fixed to 60 g, leading to a ratio between the initial fixed bed height and the reactor diameter of 0.6. The initial fluidization ratio U/U_{mf} has been fixed to 4, which corresponds to a total inlet gas flow rate of 5.33 l/min STP (slm). These two parameters have been selected to reach a good compromise between the fluidization quality (and the resulting thermal profile along the FB) and the reactor filling. Indeed, we will see that the fixed bed height sharply increases with the weight of MWCNTs formed and that the bed of powders can completely fill in the reactor after 60 or 70 min of run if the initial mass of catalytic powders is too high. On the other hand, the initial height of catalyst bed into the reactor must be high enough so that convenient thermal and mass transfers exist into the bed till the beginning of the synthesis; this will allow to rapidly reach quite isothermal conditions and then maximal productivity and selectivity in MWCNTs. As detailed in Table 1, the influences of run duration, FB temperature, inlet ethylene and hydrogen partial pressures have been studied.

Scanning electron microscopy (SEM) observations were done using a LEO-435 microscope; transmission electron microscopy (TEM) observations were conducted on a Philips CM-12 setup (120 kV in voltage) to detect the possible presence of undesired products (soot or encapsulated iron nanoparticles). Around 15 TEM micrographs were analyzed for each sample. Among them, three different magnifications were used, high magnification being used for diameters measurements and MWCNT walls observations.

Thermo gravimetric analysis (TGA) was performed to evaluate the amount of carbon deposited in each experiment and also the percentage of other forms of carbon. Those analyses were conducted under air in a Setaram-92-12 apparatus with a 10°C min^{-1} ramp between 20 and 1000°C followed by an isotherm at this temperature for 30 min. The distribution of grain diameters before and after MWCNT synthesis was measured with a Malvern-2600C laser granulometer equipped with a Sirocco-2000 sampler in dry mode.

The process efficiency was also characterized through the following parameters:

(i) the weight of produced material during each run,

(ii) the MWCNT yield R_{CNT}, corresponding to the ratio between the final MWCNT weight and the weight of injected carbon,

(iii) the process selectivity S in MWCNTs was deduced from TEM and SEM observations, Raman spectra and TGA analyses; S has been noted from * for a low selectivity, to **** for an excellent one (see Appendix Figures A1–A4 for representative examples),

(iv) the productivity X_1 defined as the mass of deposited carbon per gram of catalyst,

(v) the apparent grain density ρ_p of the MWCNT/catalyst composite material, by measuring the final fixed bed height H and the weight of the bed, assuming a constant void fraction of the fixed bed, as explained below,

(vi) the minimum fluidization velocity $U_{mf,}$ measured conventionally,[15] from pressure drop measurements at decreasing gas flow rate, after the end of each run at ambient temperature and using pure nitrogen.

Table 1. Operating Conditions Tested

Run	Weight % of Fe	T (°C)	Run duration (min)	Q_{N2} (slm)	Q_{H2} (slm)	$Q_{C_2H_4}$ (slm)
Cin1	10	650	120	1.33	1.33	2.66
Cin2			105			
Cin3			90			
Cin4			60			
Cin5			30			
Cin6			10			
Cin7	10	550	90	1.33	1.33	2.66
Cin8		600				
Cin9		700				
Cin10		750				
Cin11	10	650	90	2.66	1.33	1.33
Cin12				2.00		2.00
Cin13				3.00		1.00
Cin14				1.00		3.00
Cin15				1.33	2.66	1.33
Cin16					2.00	2.00
Cin17					3.00	1.00
Cin18					1.00	3.00
Cin19				1.00	1.66	2.66
Cin20				1.66	1.00	
Cin21				0.50	2.16	
Cin22				2.66	0	
Cin23	3.5	650	90	1.33	1.33	2.66
Cin24	5.0					
Cin25	13.5					
Ethane1	10	650	90	1.33	1.33	2.66
Ethane2	10	750				

Table 2. Experimental Results Obtained for Various Run Durations

Run	R_{CNT} (%)	X_1 (g_C/g_{cata})	A_1 (g_C/g_{Fe}/h)	S	H (cm)	d_P (μm)	U_{mf} (cm/s)	ρ_P (kg/m^3)	X_2 (g_C/g_{cata})	A_2 (g_C/g_{Fe}/h)	X_3 (g_C/g_{cata})	A_3 (g_C/g_{Fe}/h)
Cin1	50.0	2.7	13.3	****	76	361	4.3	74	1.07	5.4	0.24	1.2
Cin2	42.6	2.0	11.4	****	55	510	3.6	250	1.04	5.9	0.17	0.98
Cin3	45.8	1.8	12.2	****	42	564	3.1	307	0.97	6.5	0.10	0.67
Cin4	33.1	0.9	8.9	****	21	455	2.4	459	0.65	6.5	0.08	0.80
Cin5	30.8	0.4	8.3	****	9	345	1.4	895	0.28	5.6	0.04	0.80
Cin6	30.0	0.13	8.0	****	4	339	2.9	1496	0.09	5.4	0.02	1.20

It is worth noting that the MWCNTs yield R_{NCT}, and the productivity X_1 have been calculated for all runs assuming a 100% selectivity. This assumption leads to an overestimation of R_{CNT} and of X_1 for the runs presenting a lower selectivity.

Results and Discussion

The results we obtained for MWCNT production are detailed in Tables 2–5. First, for the nominal run Cin3, and according to TGA and TEM observations, the selectivity in MWCNTs has been excellent as shown in Figure 2, and neither soot nor encapsulated particle nor filament have been detected. The MWCNT yield R_{CNT} is 45.8% and the productivity in MWCNTs is 1.8 g_C/g_{cata}. These values are quite low considering, in particular, that we used a 10% Fe/Al$_2$O$_3$ w/w catalyst, and are due to the initial very low bed height. The final fixed bed height is 42 cm, corresponding to an increase

of more than 4 mm/min along this run. This impressive evolution has already been observed by some authors,[2–4] and is directly related to MWCNT formation and especially to the concomitant marked decrease of the grain density as detailed below. As illustrated by Figure 2b, the outer diameter of the MWCNTs formed is classically comprised between 10 and 20 nm.

For run Cin3, as for all the preliminary runs performed, GC analyses have revealed the presence of ethane and methane in the outlet gases, in addition to nitrogen, hydrogen and unreacted ethylene. A similar finding was reported for MWCNT synthesis,[3] as for the production of carbon nanofibers on Ni/zeolites catalysts from C$_2$H$_4$/H$_2$ feed,[16] and for ethylene decomposition on MoAl alloys.[17] Interestingly, acetylene, butadiene or benzene, typical products from the noncatalytic CVD of carbon from ethylene,[18,19] have not been detected in the outlet gases. A blank experiment (i.e. using
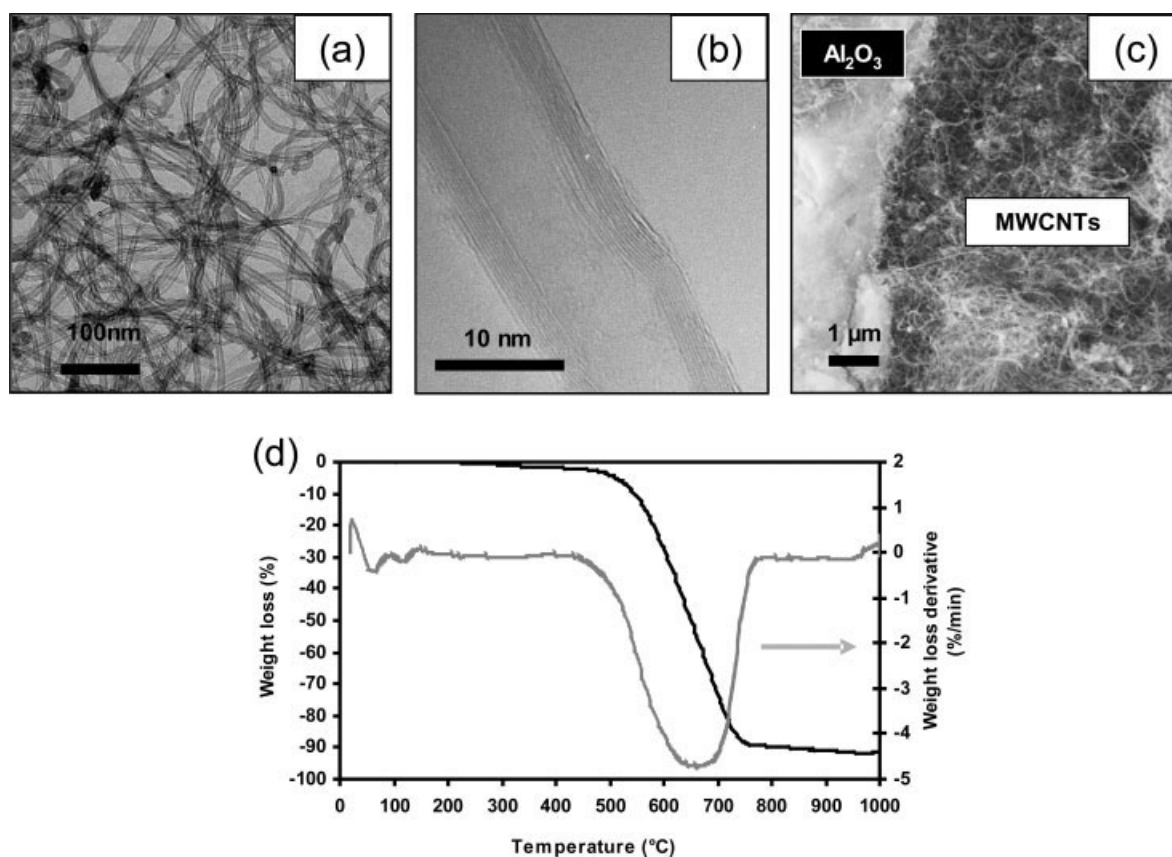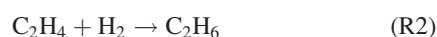

Figure 2. Characterization of materials formed after run Cin3.

(a) TEM image, (b) HREM image, (c) SEM image, and (d) TGA of the purified material.

pure alumina powders) has been performed under the conditions of run Cin3, showing that no detectable decomposition of ethylene occurs at 650°C, as found by Gommes et al.[10] Consequently, the reactions of formation of MWCNTs, ethane and methane do require the presence of the iron supported catalyst under the conditions investigated in this study. Then, the following apparent chemical scheme, composed of three apparent catalytic reactions, has been considered for the kinetic study:

$$C_2H_4 \rightarrow 2C_{CNT} + 2H_2 \qquad (R1)$$

$$C_2H_4 + H_2 \rightarrow C_2H_6 \qquad (R2)$$

$$C_2H_4 + 2H_2 \rightarrow 2CH_4 \qquad (R3)$$

It is worth noting that reaction (R_3) is the combination of two successive catalytic heterogeneous reactions, the first one being the complete or partial decomposition of ethylene in carbon or CH_x adsorbed species ($R_{3'}$) and the second one the methanation ($R_{3''}$) of the previous species containing a single carbon atom:

$$C_2H_4 \rightarrow 2CH_x + (2-x)H_2 \quad (x = 0, 1, 2) \qquad (R_{3'})$$

$$CH_x + (2 - x/2)H_2 \rightarrow CH_4 \qquad (R_{3''})$$
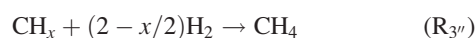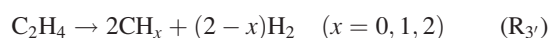
In this version of the chemical scheme, the possible formation of MWCNTs from ethane has not been considered. This path of MWCNT formation will be discussed later.

For this kinetic study, the productivity X_i (in g of carbon per gram of catalyst), has been defined for each apparent chemical reaction considered: X_1 (for MWCNT formation) has been deduced from mass balances after GC measurements and when possible has been checked by weighing, and X_2 and X_3 (respectively corresponding to ethane and methane formation) have been deduced from GC measurements. Similarly, three average activities A_i have been defined in gram of carbon per gram of iron and per hour.

The influence of the main operating parameters has been studied as detailed below. For each run, all the conditions have been kept equal to those of the nominal run Cin3 except the studied parameter.

Influence of deposition duration

As indicated in Table 1, the deposition duration has been varied between 10 and 120 min going from runs Cin1 to Cin6. It is worth noting that for run Cin1 (120 min), for which a particularly high productivity in MWCNTs has been reached, a slight de-fluidization has been observed on the temporal profiles of pressure drop and bed temperatures. Representative examples of such profiles for run Cin11 (with good fluidization conditions) and run Cin14 (with agglomeration) are given in Appendix. They indicate that when agglomeration occurs, (most often when $X_1 > 2.4$ g_C/g_{cata}), results in terms of process efficiency are clearly less precise, mostly because of the loss of convenient gas-solid contact and of bed isothermicity.

The three productivities and the final fixed bed height increase with run duration as detailed in Table 2 and illustrated in Figure 3.
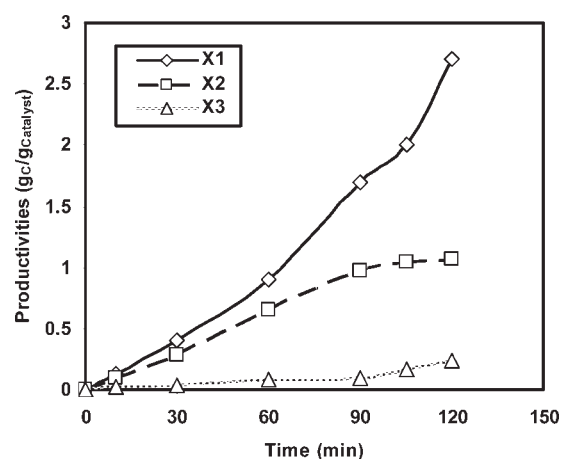

Figure 3. Influence of deposition duration on the productivities (runs Cin1 to Cin6).

It is worth noting that methane productivity X_3 is always significantly smaller than the two other productivities. No catalyst deactivation has been noticed under the investigated conditions. The productivity for the formation of MWCNTs X_1 tends to increase significantly with time-on-stream, whereas that of ethane formation X_2 remains quasi constant after 60 min of reaction. We believe that carbon deposition (R_1) is the main reason for the catalyst deactivation for ethylene hydrogenation at reaction times longer than 60 min.[20] The methanation rate weakly increases after 60 min of reaction.

For the whole conditions investigated, the selectivity in MWCNTs appears to be excellent as illustrated by the TEM micrographs of Figure 4 and by the presence of a single peak centered at 650°C on the TGA profiles.

After each run, the granulometry distribution and the minimum fluidization velocity of the composite powders have been measured and the results are given in Table 2. For some runs, the void fraction at minimum fluidization has also been measured as being close to 0.55. It was slightly affected by deposition, probably because the powders morphology remained roughly spherical at least till 90 min of run, as shown on the SEM images of Figure 5. As a consequence, the composite grain density has been calculated as a function of run duration, as detailed in Table 2 and shown on Figure 5f. It was initially equal to 1930 kg/m³ for the Fe/Al₂O₃ catalyst and decreased sharply till 60 min to 460 kg/m³, and then more slowly, to reach 74 kg/m³ at 120 min. This evolution is due to the low density of the MWCNTs produced and to the marked bed expansion occurring with run duration. The fact that the decrease of the grain density is slower during the end of the run (60–120 min), (period during which the catalyst productivity in MWCNTs increase is more pronounced), should be associated to the explosion of catalyst grains after 60 min of reaction. Indeed, we have attributed the decrease in mean particle diameter observed with run duration to an explosion of the catalyst grains due to CNT growth into the porous volume of the Al₂O₃/Fe catalyst, after 60–100 min of run. This assumption has been confirmed by many SEM views of catalyst/CNT composite grains. These SEM views are not presented in this article for confidentiality
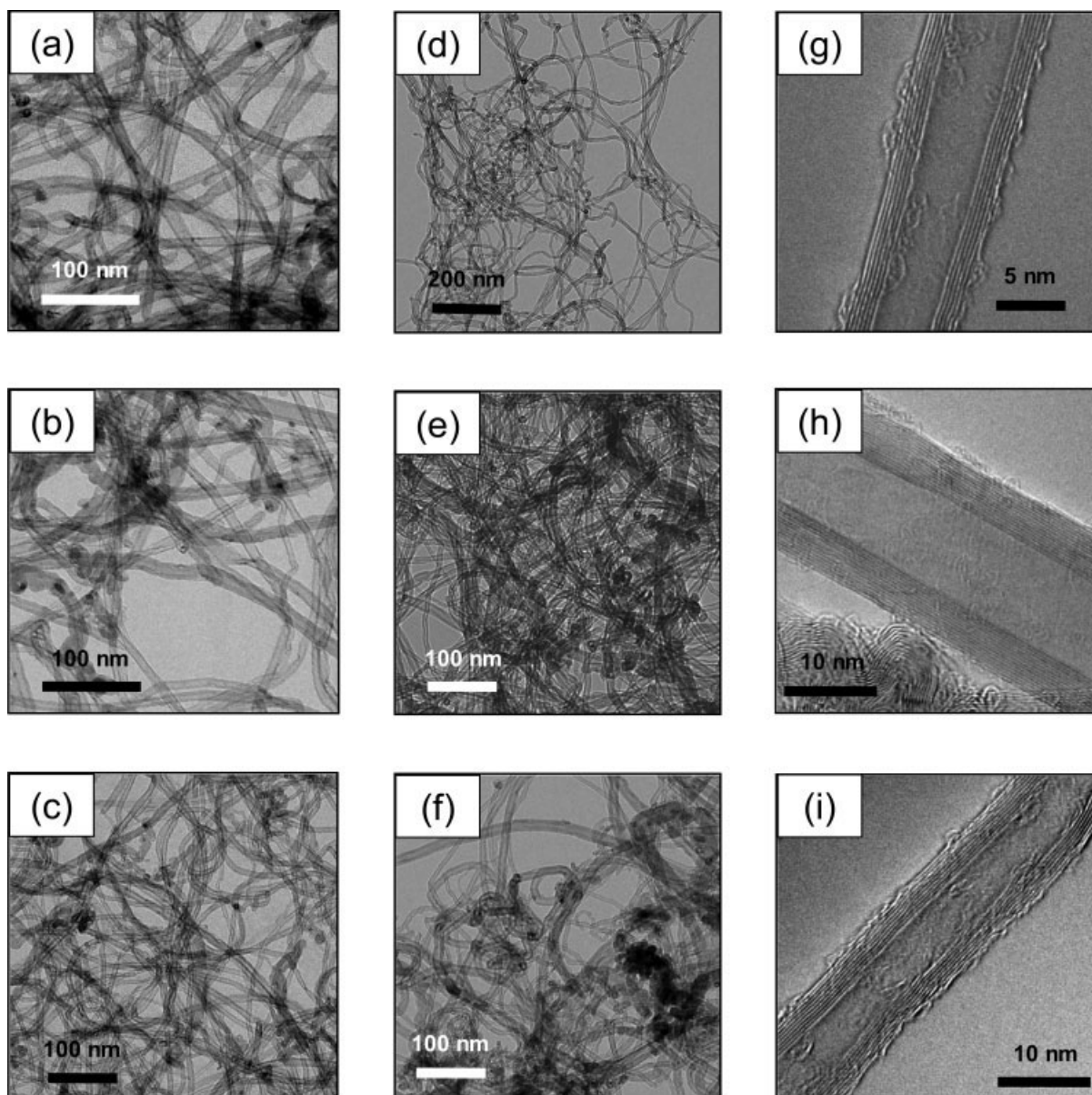
Figure 4. TEM views of products formed during runs.
(a) Cin 1, (b) Cin 2, (c) Cin3, (d) Cin4, (e) Cin5, (f) Cin6, (g) Cin3 TEM-high magnification, (h) Cin4 TEM-high magnification, and (i) Cin5 TEM-high magnification.

reasons. This explosion creates smaller grains of catalysts rich in Fe/Al_2O_3 catalyst. Concerning the mean volume diameter of grains, it can be observed in Table 2 that it increases with run duration till a critical MWCNT productivity (roughly 1.9 g_C/g_{cata} obtained at 60–100 min of deposition), from which grains seem to massively explode. These two profiles explain the evolution of the minimum fluidization velocity: indeed U_{mf} decreases with run duration till 30 min and then regularly increases, in agreement with the Ergun relation[15] for which U_{mf} depends on $d_p^3(\rho_p - \rho_g)$.

Influence of temperature

Five temperatures have been examined going from 550 to 750°C, corresponding to runs Cin7 to Cin10 and to the nominal run Cin3, as detailed in Tables 1 and 3. A moderate bed agglomeration occurred during run Cin9 and a more intense one during run Cin10. It clearly appears that between 550 and 700°C MWCNT productivity significantly increases. As illustrated on Figure 6a, a catalyst deactivation occurred during the run at 550°C, and even if it is less pronounced at 600°C too. At 750°C (run Cin10), a decrease of the activity occurred beyond 70 min, probably because of the poor fluidization quality due to more intense grain explosion at 750°C than at 700°C as detailed further. This probably explains the lower final productivity at 750°C than at 700°C. For runs Cin7 to Cin10, it is worth noting that the selectivity in MWCNTs is lower at 550, 700, and 750°C than at 600 and 650°C. At 550°C, TEM observations revealed the presence
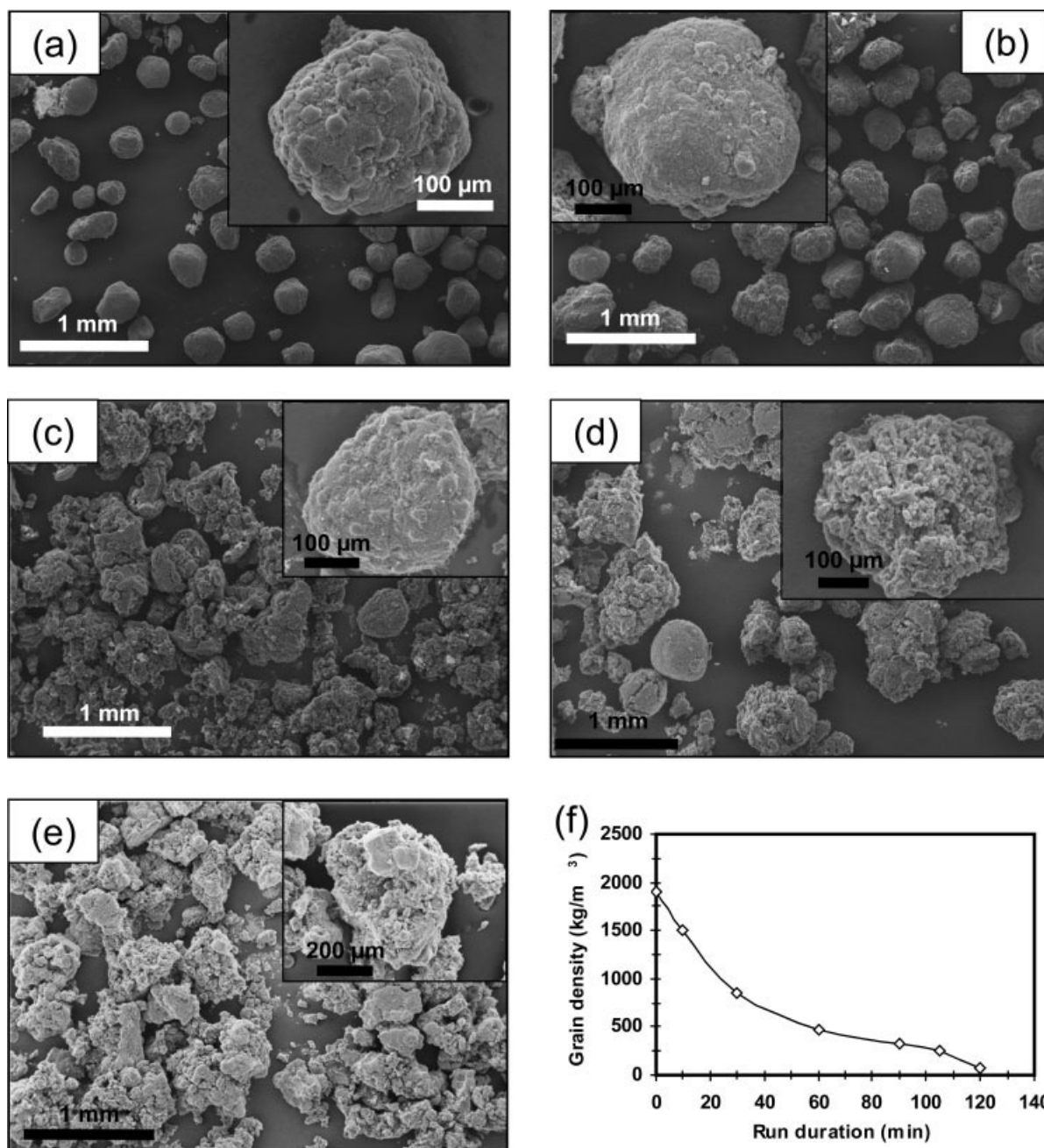
Figure 5. SEM images of powders after run.

(a) Cin6, (b) Cin5, (c) Cin4, (d) Cin3, and Cin1; and (f) evolution of powders density with run duration.

Table 3. Experimental Results Obtained for Various Temperatures

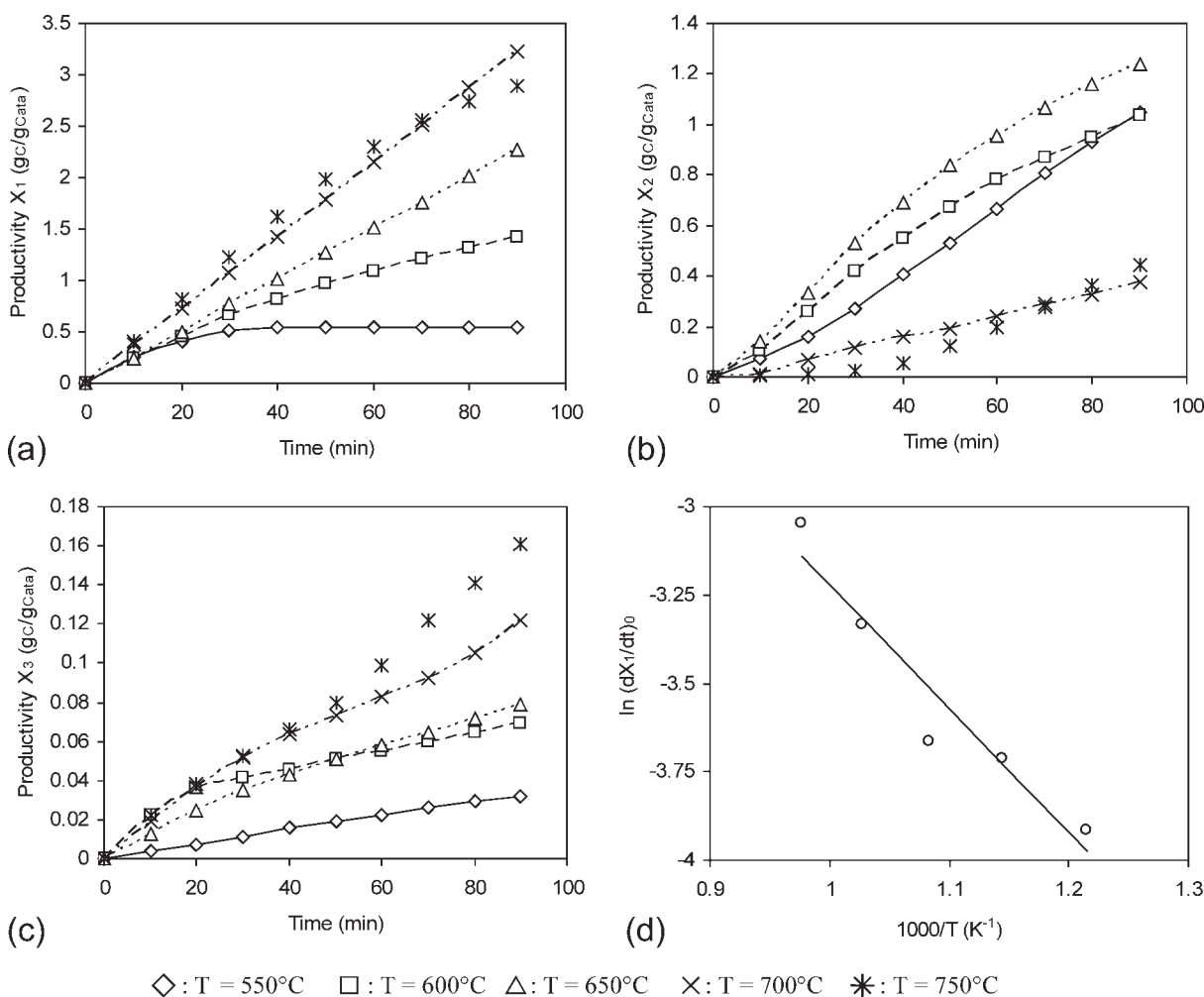| Run	R_{CNT} (%)	X_1 (g$_C$/g$_{cata}$)	A_1 (g$_C$/g$_{Fe}$/h)	S	H (cm)	d_P (μm)	X_2 (g$_C$/g$_{cata}$)	A_2 (g$_C$/g$_{Fe}$/h)	X_3 (g$_C$/g$_{cata}$)	A_3 (g$_C$/g$_{Fe}$/h)
Cin7	13.5	0.54	1.2	***	5	325	1.05	0.12	0.032	0.0036
Cin8	35.8	1.43	7.8	****	25	393	1.24	0.14	0.069	0.0077
Cin9	75.0	3.00	20	***	85	375	0.37	0.04	0.122	0.014
Cin10	70.8	2.83	18.9	***	78	304	0.44	0.05	0.161	0.018
Ethane1	2.8	0.11	0.73	**	–	–	–	–	–	–
Ethane2	27.5	1.1	7.33	***	–	–	–	–	–	–

Figure 6. (a) to (c) Influence of temperature on the productivities, (d) Initial velocity of MWCNT formation vs. the inverse of temperature (runs Cin3, Cin7 to Cin10).

of large diameter (100–200 nm) filaments and of numerous encapsulated particles; at 700 and 750°C, such filaments were also present but with less encapsulated particles. The preferential formation of large diameter CNTs at low temperature has already been reported,[3,21] and it can be due to the presence of α-Fe at these temperatures.

At 550°C, due to the low MWCNT productivity, the final granulometry of powders was close to that of the initial catalyst. At 600°C, the granulometry distribution was centered on a higher value than the initial one but presented an identical profile; this indicates a homogeneous growth of MWCNTs on all the grains without explosion. At 650 and 700°C, the mean volume diameters was close to that at 600°C; the only difference is the presence of grains of lower diameter than the initial powders, thus showing a beginning of grain explosion. The granulometry distribution at 750°C was larger than the others and revealed an important proportion of exploded grains. This behavior should be linked to the high productivity X_1 at 750°C during the first hour of reaction, **and**/or to the fast kinetics of metal dusting[22] at this temperature, leading to a more marked explosion of the catalytic grains.

For the reaction of ethane formation, two groups of curves can be observed in Figure 6b: (i) the evolution of X_2 at 550, 600, and 650°C presents similar final productivities but increasing initial slopes, and (ii) the productivities at 700 and 750°C are similar but significantly lower than the others and the initial slopes tend to decrease with temperature. According to some authors,[13,23] the decrease of X_2 for the two highest temperatures could be due to the fact that under these conditions, ethane directly forms MWCNTs. To confirm this assumption, two experiments with ethane as unique carbon source have been performed, Ethane1 and Ethane2, as detailed in Table 1. For these two runs, the gas flow rates have been fixed so as to inject the same mass of carbon as in the nominal run Cin3 (i.e. 240 g). The results obtained are presented in Table 3. At 650°C, only low amounts of MWCNTs have been produced ($X_1 = 0.11$ g_C/g_{cata}) with a poor selectivity particularly due to the presence of numerous encapsulated particles and of large diameter filaments observed by TEM.[14] At 750°C, higher productivity and selectivity in MWCNTs have been measured ($X_1 = 1.1$ g_C/g_{cata}), as detailed elsewhere.[14] So, the hypothesis of a direct contri-

Table 4. Experimental Results Obtained for Various Ethylene and Hydrogen Inlet Partial Pressures

Run	R_{CNT} (%)	X_1 (g_C/g_{cata})	A_1 (g_C/g_{Fe}/h)	S	H (cm)	d_P (μm)	X_2 (g_C/g_{cata})	A_2 (g_C/g_{Fe}/h)	X_3 (g_C/g_{cata})	A_3 (g_C/g_{Fe}/h)
Cin13	66.7	1.0	6.7	****	14	358	0.36	2.4	0.03	0.20
Cin11	54.5	1.1	7.3	***	16	424	0.48	3.2	0.06	0.40
Cin12	50.0	1.5	10.0	****	38	441	0.75	5.0	0.07	0.47
Cin14	55.6	2.5	16.7	****	75	459	1.01	6.7	0.10	0.67
Cin22	14.6	0.58	3.9	**	14	366	0.37	2.5	0.21	1.40
Cin20	31.3	1.25	8.3	****	36	594	1.03	6.9	0.087	0.58
Cin19	48.3	1.85	12.3	****	51	571	1.08	7.2	0.084	0.56
Cin21	50.0	1.90	12.7	****	60	400	1.07	7.1	0.065	0.43

bution of ethane to the formation of MWCNTs is confirmed for the highest temperatures tested.

Finally, for the reaction of methane formation (Figure 6c), the productivity X_3 and its initial slope increase with temperature. It is worth noting that whatever the temperature used, X_3 is always significantly lower than the two other productivities. In the temperature range tested, methane does not react on iron catalyst to produce MWCNTs. The irreversible formation of small amounts of methane in the system ethane-ethylene-hydrogen has already been discussed for noncatalyzed reactions, and it has been proposed that methane arises from ethylene and not from ethane decomposition.[24]

We have considered that the kinetics of the three reactions considered follow an Arrhenius law:

$$(dX_i/dt)_{t=0} = k'_{0,i} \times \exp(-E_{ai}/RT_K) \quad (1)$$

where $k'_{0,i}$ is the apparent pre-exponential coefficient for the reaction R_i and E_{ai} the apparent activation energy of reaction R_i. The whole kinetic laws have been established for the initial times of reactions. Activation energies of reactions (R_i) have been deduced from Arrhenius plots.

For MWCNT production E_{a1} is equal to 29.0 kJ/mol and the pre-exponential coefficient to 80.39 g_C/g_{cata}/h (Figure 6d). If now we consider the points $X_1(t)$ at 40 min, E_{a1} is equal to 120 kJ/mol, this value being close to those reported in the literature for MWCNT formation from ethylene.[8] The discrepancy in E_{a1} between the initial value and that at 40 min can be explained by the fact that the slopes of the curves of Figure 6a are very similar during the first 10 min. Beyond 10 min, the slopes remain constant at 650, 700, and 750°C, but those at 550 and 600°C decrease. We have seen that the catalyst grains explode during runs only between 650 and 750°C. A possible explanation for these behaviors could be that during the first 10 min of reaction, nucleation is probably the dominant mechanism for MWCNT formation, and that for the present Fe/Al$_2$O$_3$ catalyst, this initial nucleation presents low apparent activation energy. Then, nucleation continues all along the synthesis at 650°C and higher, because temperature is high enough to activate iron sites inside the catalyst grains, as proved by their explosion. On the opposite, at 550 and 600°C, only the external iron sites are active; after 10 min of run, nucleation slows down, and growth probably becomes the main mechanism of MWCNT formation. To the best of our knowledge, this is the first study highlighting the existence of two kinetic regimes for MWCNT synthesis, nucleation then growth. Such behavior of Fe/Al$_2$O$_3$ catalysts is original and is certainly due to its

mode of preparation.[14] For the subsequent parts of our work, we have kept the initial value of E_{a1} because the behavior of the process at 550 and even 600°C is clearly less interesting than at 650 and 700°C.

Now, concerning our apparent kinetic scheme, the MWCNTs produced from ethane are included in the apparent reaction (R_1) because ethane is formed from the injected ethylene. As a first approach, we have then chosen to account for the decrease of X_2 by two Arrhenius like laws. The first part of the law, between 550 and 650°C shows apparent activation energy of 17.2 kJ/mol and a pre-exponential coefficient of 7.98 g_C/g_{cata}/h and the second part has an apparent "deactivation" energy of -94.0 kJ/mol and an apparent constant of velocity of $3.22\ 10^{-6}$ g_C/g_{cata}/h. This representation is approximate; this is why a perspective of this work would be to study more precisely the influence of the main operating conditions on the three productivities using ethane as carbon source to propose a more complete and exact kinetic scheme.

For methane, E_{a3} is 17.0 kJ/mol and the pre-exponential coefficient is equal to 0.72 g_C/ g_{cata}/h. It is worth noting that the point at 550°C was not aligned with the others on the Arrhenius plot. As a consequence, it has not been taken into account for the determinations of the kinetic parameters, which will reduce the accuracy of the kinetic law for methane.

Influence of ethylene partial pressure

During runs Cin11 to Cin14, the hydrogen flow rate has been fixed to that of the nominal run Cin3 and the flow rates of ethylene and nitrogen have been varied so as to keep a constant total gas flow rate. The exact operating conditions tested are detailed in Table 1, whereas the corresponding results are presented in Table 4. The thermal and pressure drop temporal profiles for runs Cin11 and Cin14 are given in Appendix.

The temporal evolutions of the three productivities are plotted in Figure 7. For the three apparent reactions, the productivities clearly increase with ethylene partial pressure. As a consequence, the partial orders of reaction will be positive concerning ethylene for the three reactions considered.

We have assumed that the apparent initial kinetic laws for the three reactions considered can be of the following form:

$$(dX_i/dt)_{t=0} = k''_{0,i} \times (P_{0,C_2H_4})^{a_i} \quad (2)$$

In this equation, $k''_{0,i}$, the apparent constant of reaction and a_i, the apparent partial order of reaction for ethylene, are constant for the operating conditions tested. They have also been
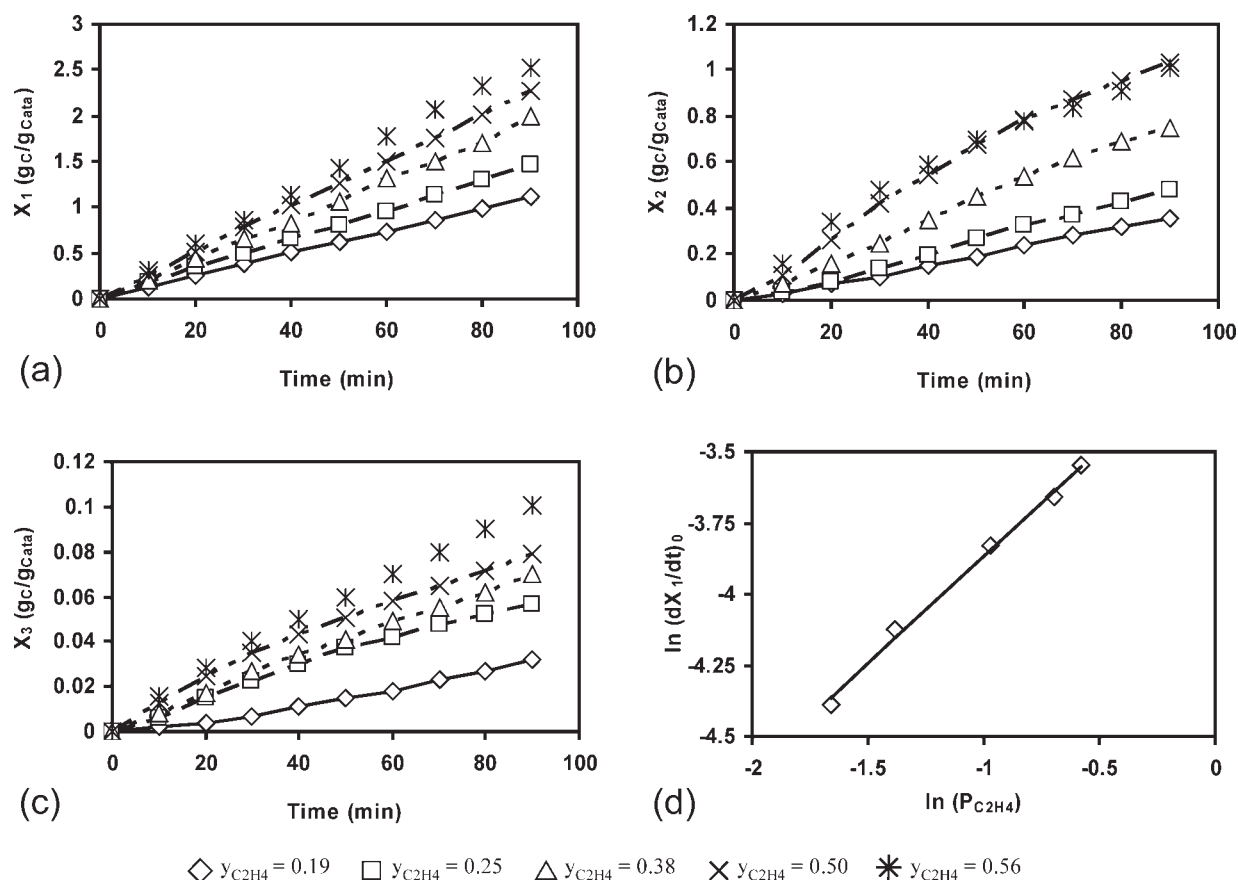
Figure 7. (a) to (c) Influence of ethylene molar fraction on the productivities, (d) Initial velocity of MWCNT formation vs. ethylene partial pressure (runs Cin3 and Cin11 to Cin14).

determined at the beginning of the reactions, since no catalyst deactivation occurred.

We have plotted in Figure 7d the logarithms of the initial velocity dX_1/dt vs. the logarithm of the inlet partial pressure of ethylene. A straight line has been obtained; its slope corresponds to the apparent partial order of the reaction. For MWCNT formation, the apparent order is 0.75, whereas a value of 0.79 has been reported for $FeCo/Al_2O_3$ catalysts at $700°C$.[8] For the reaction of ethane formation (curve not presented), the apparent order is 1, in agreement with literature results about catalytic hydrogenation of ethylene.[25,26] Finally, the apparent order for the reaction of methane formation (curve not presented) is 1.37. The apparent constants of reaction are, respectively, 2.64 $g_C/g_{cata}/bar^{0.75}/h$, 1.26 $g_C/g_{cata}/bar/h$ and 0.19 $g_C/g_{cata}/bar^{1.37}/h$ for the three reactions studied.

The final fixed bed heights logically increase with the ethylene partial pressure. The mean grains volume diameters also increase with P_{C2H4} but only till the conditions of Cin3 ($y_{C2H4} = 0.5$). For Cin14 ($y_{C2H4} = 0.56$), more massive grain explosions occurred due to intense MWCNT formation in the porous volume of the catalyst. Both the final fixed bed heights and the mean grains volume diameters are in agreement with the X_1 productivities. The selectivity in MWCNTs was excellent for the whole ethylene partial pressures tested.

Influence of hydrogen partial pressure

For runs Cin19 to Cin22, the ethylene flow rate was the same than for run Cin3 and the hydrogen and nitrogen flow rates have been varied to keep the total inlet gas flow rate constant and equal to the nominal value of 5.33 slm (Table 1). Figure 8 presents the temporal evolution of the three productivities. It can be observed that the productivity of each reaction remains in the same order of magnitude whatever the inlet molar fraction of hydrogen. But in the absence of injected hydrogen, the productivities of the reactions of MWCNTs and of ethane formation decrease whereas that of methane formation increases. This latter behavior can be explained by the fact that without added hydrogen more amorphous carbon is deposited, and consequently, more methane is produced from the hydrogen formed during the decomposition of ethylene into MWCNTs or amorphous carbon. From these results, a zero order with regard to hydrogen has been fixed for the three apparent reactions; a value close to zero was also reported for the hydrogen partial order for MWCNT growth on $FeCo/Al_2O_3$ catalysts between 600 and $700°C$.[8] In the case of R_2, a zero order for hydrogen and an order of 1 for ethylene are in agreement with a catalyst surface covered by hydride species, and thus the dissociative chemisorption of dihydrogen on iron is not rate determining. This hydride species will also be available for methane for-
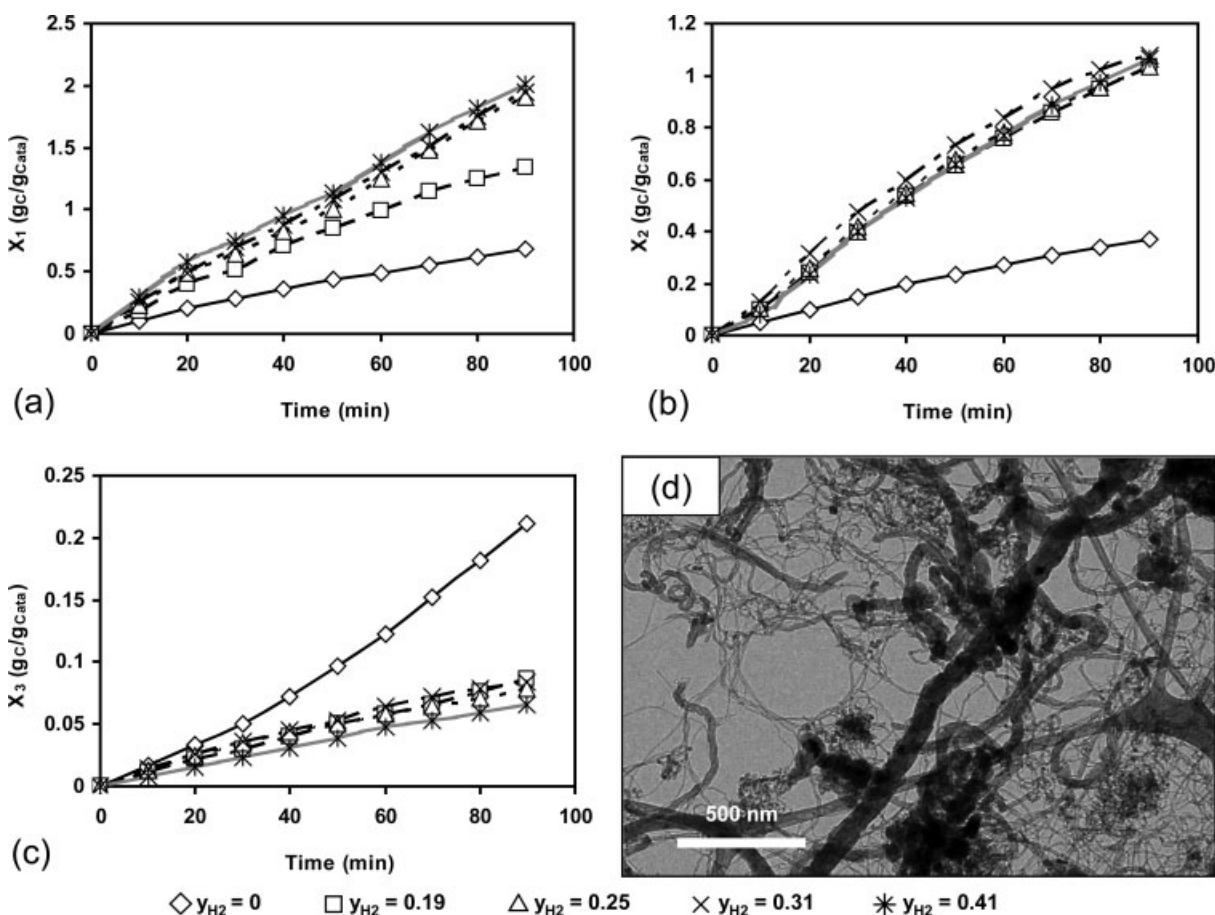
Figure 8. (a) to (c) Influence of the hydrogen molar fraction on the productivities (runs Cin3 and Cin19 to Cin22), (d) TEM image of the materials formed after run Cin22.

mation, and for R_3 the formation of surface CH_X species by C—C bond scission should be rate determining.

Runs corresponding to an inlet partial pressure of hydrogen fixed to zero will not be covered by our model and would necessitate to be treated differently. If we analyze more precisely Figure 8a, MWCNT productivities are lower for $y_{H_2} = 0.19$ than for the higher inlet molar fractions of hydrogen and they slow down with time. It is then likely that a minimum amount of hydrogen is necessary to maintain a good catalytic activity of MWCNT formation and to avoid a poisoning of the active phase. This behavior is in agreement with literature results[25,26] standing that hydrogen allows to remove amorphous carbon from the catalytic surface by methanation and thus to limit catalyst poisoning.

As detailed in Table 4, the final fixed bed height regularly increases with hydrogen partial pressure. The final mean grains volume diameter increases with the inlet hydrogen molar fraction till $y_{H_2} = 0.19$ (runs Cin22 and Cin20) and then tends to decrease due to the intense MWCNT formation rate and the related grain explosions. Both the final fixed bed heights and the mean grains volume diameters are in agreement with the X_1 productivities, if compared with the values obtained during the study on the run duration influence.

TEM analyses revealed that the selectivity in MWCNTs was excellent for all experiments except for run Cin22 without hydrogen, for which carbon filaments, pyrolytic carbon, and encapsulated particles were also produced. These results confirm the major role of hydrogen under the conditions tested, to limit the formation of carbon by-products.

Influence of iron loading

Runs Cin23 to Cin25 have been performed using Fe/Al_2O_3 catalysts with, respectively, iron loadings of 3.5, 5, and 13.5% w/w (Table 1). The granulometry of these catalysts was identical to that of the nominal one at 10 wt % of Fe. Table 5 and Figure 9a present the influence of the iron loading on the three final productivities for these experiments and for run Cin3.

The productivities of the reactions of MWCNT production and in a lesser extent, of ethane formation tend to increase with the iron loading. These evolutions are not proportional to the iron content increase, probably because the amount of injected carbon remains constant, leading to a default in carbon precursor by comparison with the amount of active phase and then probably to a lowering of the catalytic performances. An opposite trend is observed for the methane

Table 5. Experimental Results Obtained for Various Catalyst Iron Loadings

Run	R_{CNT} (%)	X_1 (g_C/g_{cata})	A_1 (g_C/g_{Fe}/h)	S	H (cm)	d_P (μm)	X_2 (g_C/g_{cata})	A_2 (g_C/g_{Fe}/h)	X_3 (g_C/g_{cata})	A_3 (g_C/g_{Fe}/h)
Cin23	33.33	1.33	25.4	***	25	409	0.86	16.4	0.162	3.08
Cin24	41.7	1.66	22.2	***	35	415	0.88	11.7	0.135	1.80
Cin25	50.0	2	9.88	****	60	388	1.02	5.03	0.097	0.48

formation, and X_3 slightly decreases with the iron content. This seems logical because the ratio between the carbon injected and the amount of iron decreases, thus allowing limiting the formation of amorphous carbon per catalytic site. Another time, X_3 is always significantly lower than the two other productivities. These results show that the iron loading has no significant influence on X_2 and X_3.

On Figure 9b has been plotted, the evolution of the logarithm of the initial velocities dX_1/dt vs. the logarithm of the weight of iron. The slope of the straight line obtained is 0.28.

As indicated in Table 5, the selectivity in MWCNTs is excellent for the two highest iron loadings tested. For the two lowest ones (runs Cin23 and Cin24), TEM analyses indicated the presence of some encapsulated particles, carbon filaments and amorphous carbon. This slight loss of selectivity can be explained by a too high carbon supply in comparison with the active phase. The presence of these carbon by-products is in agreement with the slightly higher productivities of methane formation obtained during these runs.

Conclusions

Multi-walled carbon nanotubes can be produced selectively in a fluidized bed reactor by reaction of C_2H_4/H_2 mixtures at 650°C on a 10% w/w Fe/Al_2O_3 catalyst. For the whole conditions tested, the catalyzed decomposition of ethylene produces MWCNTs, hydrogen, ethane, and methane. Above 650°C, ethane itself produces significant amounts of MWCNTs, whereas methane does not react in the temperature range 550–750°C.

In the 650–750°C range, no deactivation of the catalyst has been observed because nucleation occurs all along run duration; this is due to the activation of iron sites inside the catalyst grains porosity as proved by grains explosion during the runs. The selectivity of the process is excellent at 600 and 650°C. The formation of MWCNTs induces a marked bed expansion and a sharp decrease of grain density. Good fluidization conditions have been observed for all the conditions tested except after 70 min at 750°C of reaction, due to a more intense grain explosion.

An apparent activation energy of 29 kJ/mol has been obtained for MWCNTs formation for the initial times of synthesis, whereas a more classical value of 120 kJ/mol has been calculated for 40 min of run. This discrepancy is due to the fact that the initial mechanisms of nucleation and to a lesser extent growth, for this catalyst require low activation energy. The situation changes after the first 10 min of run because nucleation clearly slows down at 550 and even 600°C, contrarily to what happens at higher temperature. This original behavior is probably due to the mode of preparation of the catalyst. The apparent partial order of reaction for ethylene is 0.75. No influence of hydrogen partial pressure has been evidenced provided that hydrogen was present in inlet.

The apparent initial kinetic laws for MWCNT, ethane and methane formation finally deduced from these experimental results are respectively equal to:

$$(dX_1/dt)_{t=0} = 69.97 \times (\%_{Fe} \times m_{cata})^{0.28}$$
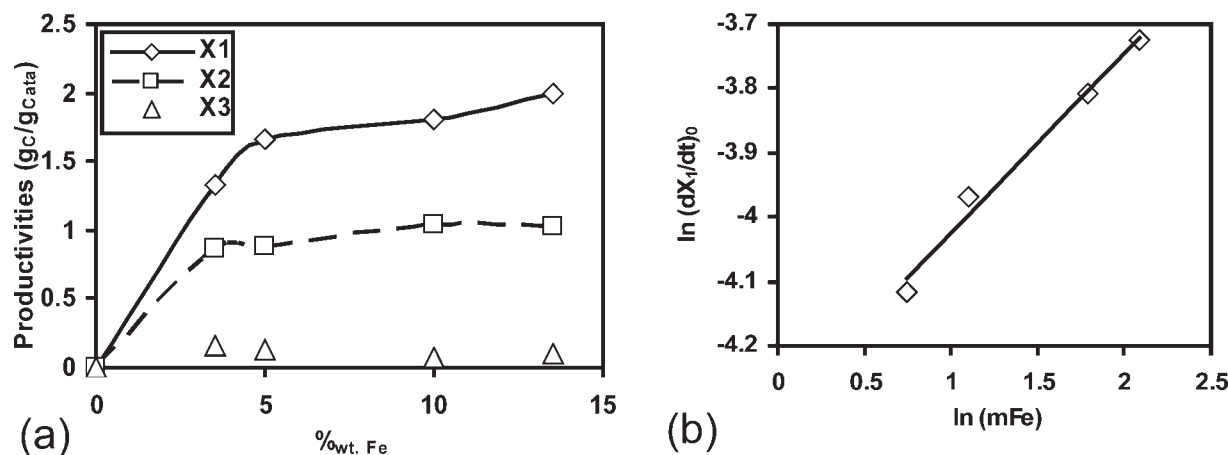$$\times \exp(-29,000/RT_K) \times (y_{C_2H_4})^{0.75} \quad (3)$$

Figure 9. (a) Influence of the iron weight percentage on the productivities, (b) Initial velocity of MWCNT formation vs. the iron weight (runs Cin3 and Cin 23 to Cin25).

Between 550 and 650°C:

$$(dX_2/dt)_{t=0} = 15.95 \times \exp(-17,200/RT_K) \times (y_{C_2H_4})^{1.00} \quad (4)$$

Between 651 and 750°C:

$$(dX_2/dt)_{t=0} = 6.44 \times 10^{-6} \times \exp(94,000/RT_K) \times (y_{C_2H_4})^{1.00} \quad (5)$$

$$(dX_3/dt)_{t=0} = 1.76 \times \exp(-17,000/RT_K) \times (y_{C_2H_4})^{1.37} \quad (6)$$

They are not accounting for any deactivation phenomenon, so they will be more precise at 650°C and higher, than at 550 and 600°C. In the second part of the study, these laws have been implemented in a bubbling bed model to numerically simulate the process behavior.

Notation

a_i = apparent partial order of reaction (R_i) regarding ethylene partial pressure (−)
A_i = activity for reaction (R_i) (g_C/g_{Fe}/h)
d_P = volume mean diameter of particles (μm)
E_{ai} = apparent activation energy of reaction (R_i) (kJ/mol)
H = final fixed bed height (cm)
$k'_{0,i}, k''_{0,i}$ = pre-exponential coefficient for the reaction (R_i) (g_C/g_{cata})
m_{cata} = weight of catalyst into the bed (g)
$P_{0,i}$ = initial partial pressure of species i (Bar)
Q_i = inlet flow rate of the gaseous species i (l/min STP or slm)
R = constant of perfect gases (8.32 J/(mol K))
R_{CNT} = MWCNT yield (%)
S = selectivity of the process (from *: low selectivity, to ****: excellent selectivity)
t = time (s)
T = bed temperature (°C)
T_K = bed temperature (K)
U = superficial velocity of fluidization (cm s^{-1})
U_{mf} = minimum velocity of fluidization (cm s^{-1})
X_i = productivity for reaction (R_i) (g_C/g_{cata})
y_i = molar fraction of the species i (−)
ρ_g = gas density (kg/m^3)
ρ_p = apparent catalyst/MWCNT composite grain density (kg/m^3)

Literature Cited

1. See CH, Harris AT. A review of carbon nanotube synthesis via fluidized bed chemical vapour deposition. *Ind Eng Chem Res*. 2007; 46:997–1012.
2. Philippe R, Morançais A, Corrias M, Caussat B, Kihn Y, Kalck P, Plee D, Gaillard P, Bernard D, Serp P. Catalytic production of carbon nanotubes by fluidized bed chemical vapor deposition. *Chem Vap Deposition*. 2007;13:447–457.
3. Morançais A, Caussat B, Kihn Y, Kalck P, Plee D, Gaillard P, Bernard D, Serp P. A parametric study of the large scale production of multi-walled carbon nanotubes by fluidized bed catalytic chemical vapour deposition. *Carbon*. 2007;45:624–635.
4. Corrias M, Caussat B, Ayral A, Durand J, Kihn Y, Kalck P, Serp P. Carbon nanotubes produced by fluidized bed catalytic CVD: first approach of the process. *Chem Eng Sci*. 2003;58:4475–4482.
5. Qian W, Wei F, Wang Z, Liu T, Yu H, Luo G, Xiang L, Deng X. Production of carbon nanotubes in a packed and a fluidized bed. *AIChE J*. 2003;49:619–625.
6. Brukh R, Mitra S. Mechanism of carbon nanotube growth by CVD. *Chem Phys Lett*. 2006;424:126–132.
7. Endo H, Kuwana K, Saito K, Qian D, Andrews R, Grulke EA. CFD prediction of carbon nanotube production rate in a CVD reactor. *Chem Phys Lett*. 2004;387:307–311.
8. Pirard SL, Douven S, Bossuot C, Heyen G, Pirard JP. A kinetic study of multi-walled carbon nanotube synthesis by catalytic chemical vapour deposition using a Fe-Co/Al$_2$O$_3$ catalyst. *Carbon*. 2007; 45:1167–1175.
9. Zavarukhin SG, Kuvshinov GG. The kinetic model of formation of nanofibrous carbon from CH$_4$-H$_2$ mixture over a high-loaded nickel catalyst with consideration for the catalyst deactivation. *Appl Catal A: Gen*. 2004;272:219–227.
10. Gommes C, Blacher S, Bossuot C, Marchot P, Nagy JB, Pirard JP. Influence of the operating conditions on the production rate of multi-walled carbon nanotubes in a CVD reactor. *Carbon*. 2004;42: 1473–1482.
11. Kim KE, Kim KJ, Jung WS, Bae SY, Park J, Choi J, Choo J. Investigation on the temperature-dependent growth rate of carbon nanotubes using chemical vapour deposition of ferrocene and acetylene. *Chem Phys Lett*. 2005;401:459–464.
12. Perez-Cabero M, Romeo E, Royo C, Monzon A, Guerrero-Ruiz A, Rodriguez-Ramos I. Growing mechanism of CNTs: a kinetic approach. *J Catal*. 2004;224:197–205.
13. Svreck V, Kleps I, Cracioniou F, Paillaud JL, Dintzer T, Louis B, Begin D, Pham-Huu C, Ledoux MJ. Monitoring the chemical vapor deposition growth of multiwalled carbon nanotubes by tapered element oscillating microbalance. *J Chem Phys*. 2006;124: 184705.
14. Philippe R, Caussat B, Plee D, Kalck P, Serp P. French patent FR07 52711.
15. Kunii D, Levenspiel O. *Fluidization Engineering*, 2nd ed. New York: Wiley, 1991.
16. Romero A, Garrido A, Nieto-Márquez A, de la Osa AR, de Luca A, Valverde JL. The influence of operating conditions on the growth of carbon nanofibers on carbon nanofiber-supported nickel catalysts. *Appl Catal A: Gen*. 2007;319:246–258.
17. Gao F, Wang Y, Burkholder L, Tysoe WT. The chemistry of ethylene on MoAl alloy thin films formed on dehydroxylated alumina: hydrogenation, dehydrogenation and H-D exchange reactions. *Surf Sci*. 2006;600:1837–1848.
18. Norinaga K, Deutschmann O, Hüttinger KJ. Analysis of gas phase compounds in chemical vapor deposition of carbon from light hydrocarbons. *Carbon*. 2006;44:1790–1800.
19. Becker A, Hüttinger KJ. Chemistry and kinetics of chemical vapour deposition of pyrocarbon—II. Pyrocarbon deposition from ethylene, acetylene and 1,3-butadiene in the low temperature regime. *Carbon*. 1998;36:177–199.
20. Lojewska J, Makowski W, Dziembaj R. Retarding, blocking and activating the cobalt catalyst by carbonaceous deposits formed in hydrogenation of ethylene. *Chem Eng J*. 2002;90: 203–208.
21. Gozzi D, Iervolino M, Latini A. The thermodynamics of the transformation of graphite to multiwalled carbon nanotubes. *J Am Chem Soc*. 2007;129:10269–10275.
22. Szakalos P. Mechanism and driving forces of metal dusting. *Mater Corros*. 2003;54:752–762.
23. Gulino G, Veira R, Amadou J, Nguyen P, Ledoux MJ, Galvagno S, Centi G, Pham-Huu C. C$_2$H$_6$ as an active carbon source for a large scale synthesis of carbon nanotubes by chemical vapor deposition. *Appl Catal A: Gen*. 2005;279:89–97.
24. Danby CJ, Spall BC, Stubbs FJ, Hinshelwood C. The irreversible formation of methane in the system ethane-ethylene-hydrogen. *Proc R Soc Lond A*. 1953;450–464.
25. Caldin SM, Boudina M, Grant DM, Walker GS. The effect of processing conditions on carbon nanostructures formed on an iron-based catalyst. *Carbon*. 2006;44:2273–2280.
26. Yu Z, Chen D, Tøtdal B, Zhao T, Dai Y, Yuan W, Holmen A. Catalytic engineering of carbon nanotube production. *Appl Catal A: Gen*. 2005;279:223–233.
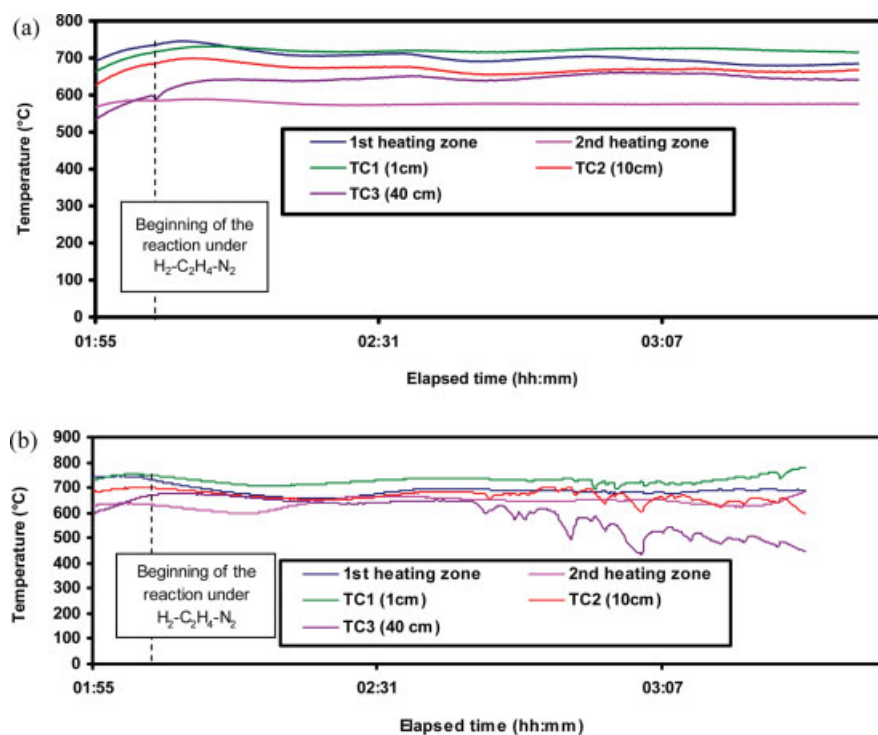
Appendix

Figure A1. Temporal evolution of thermal profiles during runs.

(a) Cin11 and (b) Cin14. [Color figure can be viewed in the online issue, which is available at www.interscience.wiley.com.]
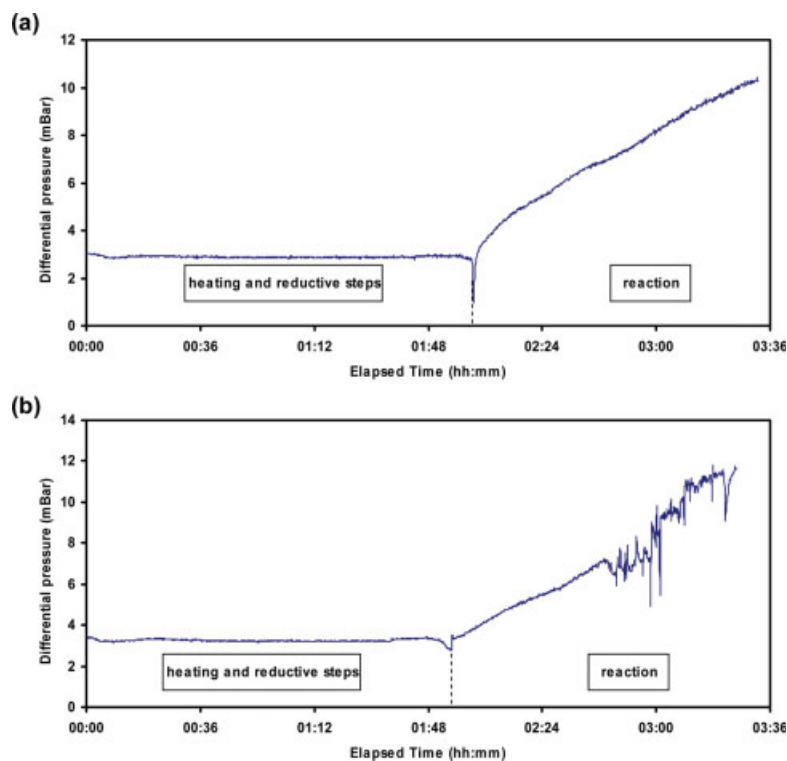

Figure A2. Temporal evolution of bed pressure drop during runs.

(a) Cin11 and (b) Cin14. [Color figure can be viewed in the online issue, which is available at www.interscience.wiley.com.]
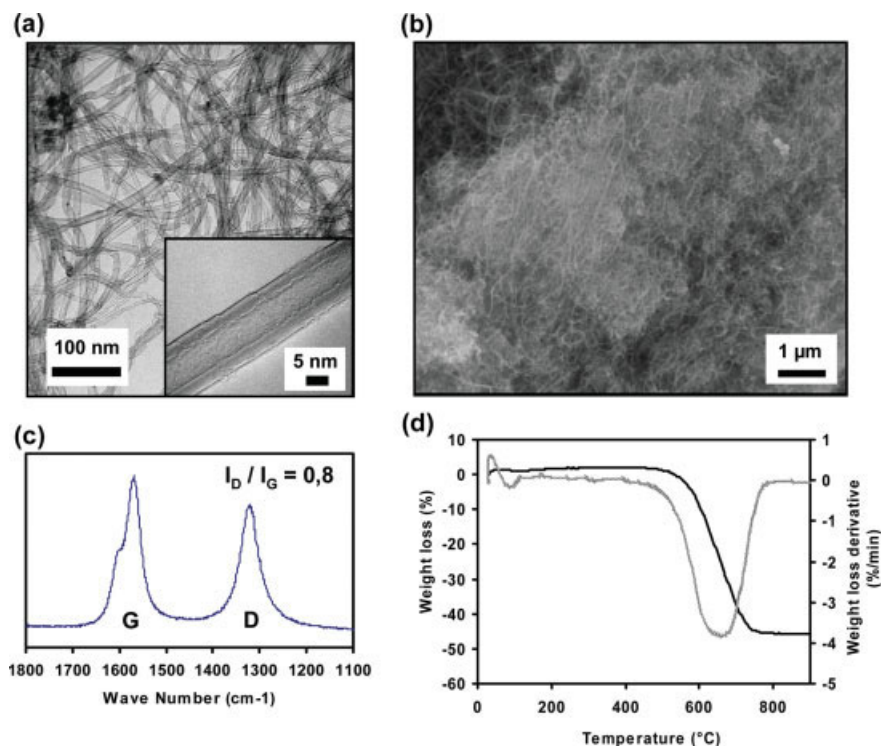
Figure A3. Characterizations used to analyze the process selectivity for run Cin13 (excellent selectivity **).**

(a) TEM micrography (b) SEM micrography (c) Raman Spectroscopy (d) ATG/DTG. [Color figure can be viewed in the online issue, which is available at www.interscience.wiley.com.]
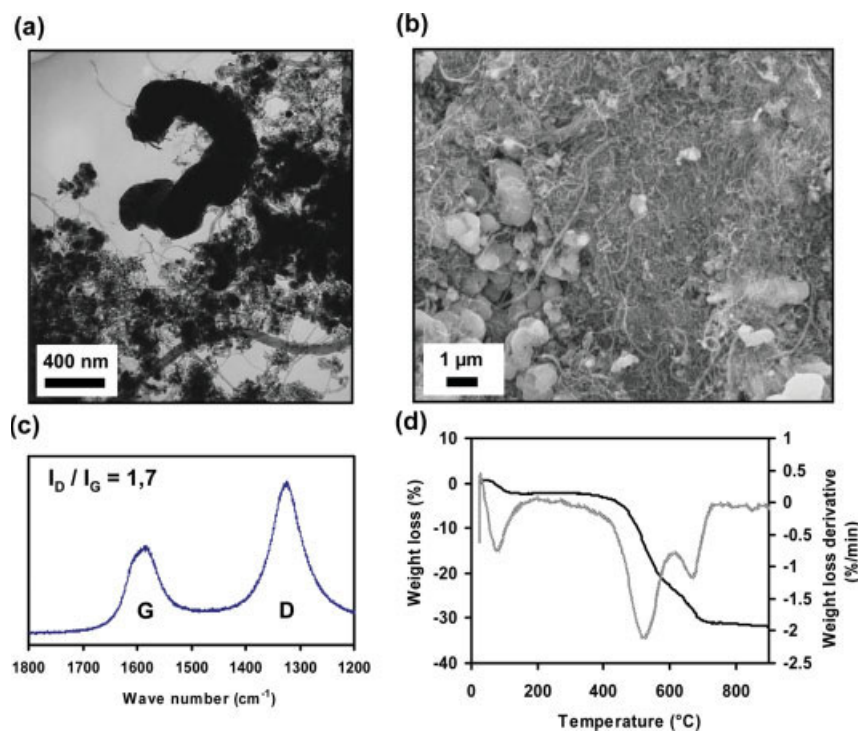

Figure A4. Characterizations used to analyze the process selectivity for run Cin22 (medium selectivity **).

(a) TEM micrography (b) SEM micrography (c) Raman Spectroscopy (d) ATG/DTG. [Color figure can be viewed in the online issue, which is available at www.interscience.wiley.com.]